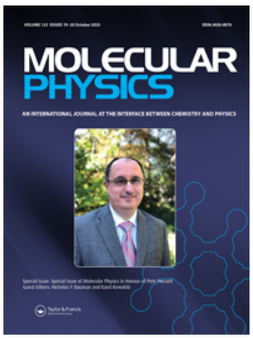

Taylor & Francis
Taylor & Francis Group

Molecular Physics

An International Journal at the Interface Between Chemistry and Physics

ISSN: 0026-8976 (Print) 1362-3028 (Online) Journal homepage: www.tandfonline.com/journals/tmph20

Infrared photoionisation of neutral tantalum and tantalum oxide clusters

Peter D. Watson, Ruby G. Spratt, Philip A. J. Pearcy, Peter T. Rubli, Christian T. Haakansson, Joost M. Bakker & Stuart R. Mackenzie

To cite this article: Peter D. Watson, Ruby G. Spratt, Philip A. J. Pearcy, Peter T. Rubli, Christian T. Haakansson, Joost M. Bakker & Stuart R. Mackenzie (12 Dec 2025): Infrared photoionisation of neutral tantalum and tantalum oxide clusters, Molecular Physics, DOI: 10.1080/00268976.2025.2596916

To link to this article: https://doi.org/10.1080/00268976.2025.2596916

MOLECULAR PHYSICS e2596916
https://doi.org/10.1080/00268976.2025.2596916

Taylor & Francis
Taylor & Francis Group

SPECIAL ISSUE IN HONOUR OF FREDERIC MERKT

Infrared photoionisation of neutral tantalum and tantalum oxide clusters

Peter D. Watson [a], Ruby G. Spratt [a], Philip A. J. Pearcy [a], Peter T. Rubli [a], Christian T. Haakansson [a], Joost M. Bakker [b,c] and Stuart R. Mackenzie [a]

[a]Chemistry Research Laboratory, Department of Chemistry, University of Oxford, Oxford, UK; [b]HFML-FELIX, Nijmegen, The Netherlands; [c]Institute for Molecules and Materials, Radboud University, Nijmegen, The Netherlands

ABSTRACT

Resonant and non-resonant multiple photon excitation of small tantalum and tantalum oxide clusters, Ta_nO_m ($n = 4$–15, $m = 0, 1, 2$) is shown to lead to thermionic emission and the production of the corresponding cationic clusters. In this way, we have recorded mass-resolved photoionisation spectra in the mid-infrared using the intense free-electron laser for intracavity experiments (FELICE). All spectra exhibit a broad non-resonant band with lower thresholds around 800 cm^{-1} whose efficiency increases to higher wavenumbers as fewer photons are required to reach the ionisation threshold. In addition, the neutral oxide clusters have strong resonant absorptions feature assigned as the oxide symmetric stretching mode, and their infrared spectra are very similar to those reported previously for the corresponding cationic clusters, $Ta_nO_m^+$, recorded by infrared multiple photon dissociation.

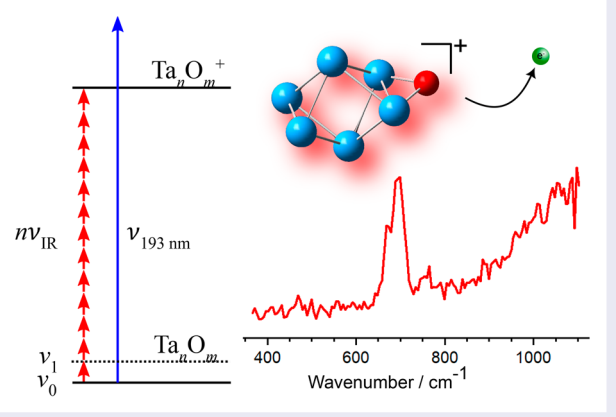

ARTICLE HISTORY
Received 8 October 2025
Accepted 25 November 2025

KEYWORDS
Metal clusters; infrared multiple photon ionisation; thermionic emission; mass spectrometry; electronic spectroscopy

1. Introduction

Refractory metals (W, Nb, Ta) exhibit physical and photochemical properties unusual amongst the transition metals, being typically hard, with high melting points and low work functions. Tantalum has a particularly high melting point (3290 K) [1] and density (16.6 g/cm^3) [1], as well as a work function of just 4.352 ± 0.001 eV (211 crystal) [2]. These metals undergo thermionic emission at high temperatures while preserving structural stability giving rise to their application as cathode materials in electron emitting devices such as filament bulbs, electron microscopes, and electron ionisation sources [3].

Isolated metal clusters represent attractive models systems to understand the evolution of physical and electronic properties with cluster size [4]. Tantalum clusters show strong catalytic activity/molecular activation towards a number of small molecules, as reviewed by Heiz and coworkers [5]. Notably, even at cryogenic temperatures, cationic tantalum clusters (Ta_n^+) dissociate multiple N_2 molecules forming polynitrides ($Ta_nN_{0,2,4}^+$), despite no such reaction proceeding on bulk tantalum [6,7]. The reactions of the monomer cation, Ta^+, towards small hydrocarbons (particularly CH_4) have been studied extensively by the groups of

CONTACT Stuart R. Mackenzie stuart.mackenzie@chem.ox.ac.uk Chemistry Research Laboratory, Department of Chemistry, University of Oxford, Mansfield Road, Oxford OX1 3TA, UK

Supplemental data for this article can be accessed online at https://doi.org/10.1080/00268976.2025.2596916.
Experimental data contained in this article are freely available from the Oxford Research Archive (DOI: https://dx.doi.org/10.5287/ora-mzedo2yky).

Freiser [8], Beauchamp [9], Maître [10] and Armentrout [11] in selected ion flow tube (SIFT) and guided ion beam (GIB) studies. More recently Meyer and co-workers have studied the reactions of Ta^+ with CH_4 [12,13] and CO_2 [14] in crossed-beam experiments employing velocity map imaging detection. In both cases the reaction is endothermic on the ground state $^5Ta^+$ surface and is believed to proceed via surface hopping to a low-lying $^3Ta^+$ surface, thus representing an example of two-state reactivity [13,15].

Small refractory metal clusters have also been studied spectroscopically. Hackett *et al.* used non-resonant single (220 nm) and two-photon (351, 308, and 248 nm) excitation to explore competing photoionisation and photofragmentation processes in W_n, Ta_n, and Nb_n clusters [16,17]. This work was extended to investigate delayed photoionisation, establishing both the vibrational temperatures of the clusters and the delayed ionisation kinetics [18]. Bernstein studied the single-photon ionisation of niobium and tantalum oxide clusters at different UV/VUV wavelengths and also observed delayed fragmentation [19]. Thermionic emission has been observed in cationic refractory metal clusters. Janssens and coworkers characterised radiative cooling and photofragmentation effects in Nb_n^+ ($n = 8$–22) clusters [20] and broad, non-resonant absorption and/or photofragmentation was observed in spectra of $[Ta_4(N_2)_{3-5}]^+$, Ta_{17}^+, $Ta_8O_{1-2}^+$ and $Ta_{11}O_{0-2}^+$ recorded by Niedner-Schatteburg [7] and some Ta_n^+ ($n = 6$–20) and $Ta_nO_{0-2}^+$ ($n = 6$–11) clusters by Fielicke *et al.* [21,22]. Rich electronic structure around the dissociation threshold makes accurate determination of cluster oxide ionisation energies challenging [23,24].

Structurally, refractory metal clusters have been studied by matrix isolation IR spectroscopy (Ta_4) [25] and, especially, by infrared multiple photon dissociation (IRMPD) studies, typically with free-electron laser infrared sources [4]. In each of these cases, the light source and process of ionisation leads to a number of similar spectroscopic processes variously known as IR-induced thermionic emission, IR- (resonance enhanced) multiple photon ionisation (RE)MPI and IR photoionisation, as well as IR(M)PD. Fielicke *et al.* have reported a series of fundamental IRMPD studies of $Nb_{5-9}^{0/+}$ [26], $Nb_9Ar_{1-4}^0$ [27], $Nb_{2-8}O_{4-20}^+$ [28], Ta_{6-20}^+ and $Ta_{6-11}O_{0-2}^+$ clusters [21,22]. Bakker and coworkers applied similar techniques to larger niobium clusters, Nb_{5-20} [29] (observing resonant far-IR driven thermionic emission), as well as the corresponding carbides, Nb_nC_m [30]. The same group investigated the effect of IR excitation prior to UV photoionisation [31]. We have also characterised the clusters of $TaO_2(CO_2)_n$ complexes by IRPD [32]. Typically, spectroscopic studies of this kind are assigned using structures and properties from density functional theory (DFT) simulations [33,34,35]. Ta and other refractory metals immediately form 3D structures from $n \geq 4$, and adopt bcc-like arrangements similar to the bulk [34].

The reactivity of refractory metals and their propensity for forming surface nitrides and oxides, raises the work function of the bulk material poisoning the thermionic emission capabilities required for electron emitting devices [3,36]. Hence, tantalum electron sources typically operate at high temperature and under high vacuum. Better characterisation of the nitrides and oxides may present avenues for cathode designs that leverage these unique properties.

Here, we present a combined mass spectrometric and free-electron laser multiple photon ionisation study of neutral tantalum clusters and their oxides (Ta_nO_m; $n = 4$–15, $m = 0, 1, 2$). The overall ionisation process is greatly enhanced in resonance with an optically allowed (vibrational) absorption making the ionisation yield useful for action spectroscopy. We interpret the results using corresponding known spectra and structures of the cationic clusters [35] as well as DFT calculations.

2. Experimental and computational methods

The experimental work presented here was undertaken at HFML-FELIX in the Netherlands using the molecular beam instrument coupled to the Free-Electron Laser for Intra-Cavity Experiments (FELICE). The end station has been described in detail previously [37,38]. In brief, metal clusters are generated utilising a purpose-built laser vaporisation source with a rotating tantalum rod housed in a 60 mm long, 3 mm diameter clustering channel. The rod is ablated by a pulsed Nd:YAG laser (20 Hz, *ca.* 20–30 mJ/pulse) in the presence of a pulsed expansion of a 10% Ar in He gas mixture. Once formed, clusters enter a 45 mm long cooling channel with a final 0.7 mm converging–diverging nozzle whose temperature was maintained in these experiments between 213 and 223 K using a cartridge heater and flowing liquid N_2. It is assumed that clusters thermalise to this temperature before final expansion creating a molecular beam. To generate Ta_nO_x species, 5% O_2 in He is introduced directly into the clustering channel via a secondary pulsed valve.

The resulting molecular beam, with neutral Ta_nO_m clusters entrained, is skimmed and intersected with an infrared pulse from FELICE before charged clusters are extracted into a reflectron time-of-flight (ReToF) mass spectrometer. The FELICE beam consists of 10 µs macropulses comprising ps-long micropulses each separated by 1 ns, with a transform-limited spectral

width amounting to about 0.7% of the central frequency (FWHM). The peak intracavity macropulse energy (reconstructed from a fraction of light outcoupled) during these experiments was 0.86 J at 1300 cm^{-1}. To exclude cationic clusters produced by the (grounded) source, the skimmer was typically held at +100 V. To account for long-term source drift in the generation of the neutral clusters, an ArF eximer laser (193 nm, 10 Hz) is pulsed on alternate gas pulses to the FELICE beam to record single photon ionisation reference mass spectra. IR photoionisation spectra are recorded as relative enhancement cross-sections of $Ta_nO_m^+$ species as a function of photon energy ($\sigma = \frac{1}{\varphi}\frac{N_f}{N_0}$; where φ is the macropulse photon flux, N_f is the mass spectrum intensity with the FELICE beam and N_0 is the reference mass spectrum intensity following 193 nm ionisation).

To complement the experimental spectra, energetically low-lying cluster structures are calculated with density functional theory using UB3P86/def2TZVP [39] methods in Gaussian16 [40]. The UB3P86 functional is chosen for its low computational cost and demonstrated performance in cluster calculations in previous work from both this group [38,41,42] and others [43]. Literature structures for Ta_{2-14} were used as initial structural starting points [35], reoptimised and their harmonic frequencies calculated. For oxide doping, the stochastic *Kick*[3] algorithm is used to decorate the surface of the cluster, with sufficiently large sampling and reoptimisation yielding optimised structures [44].

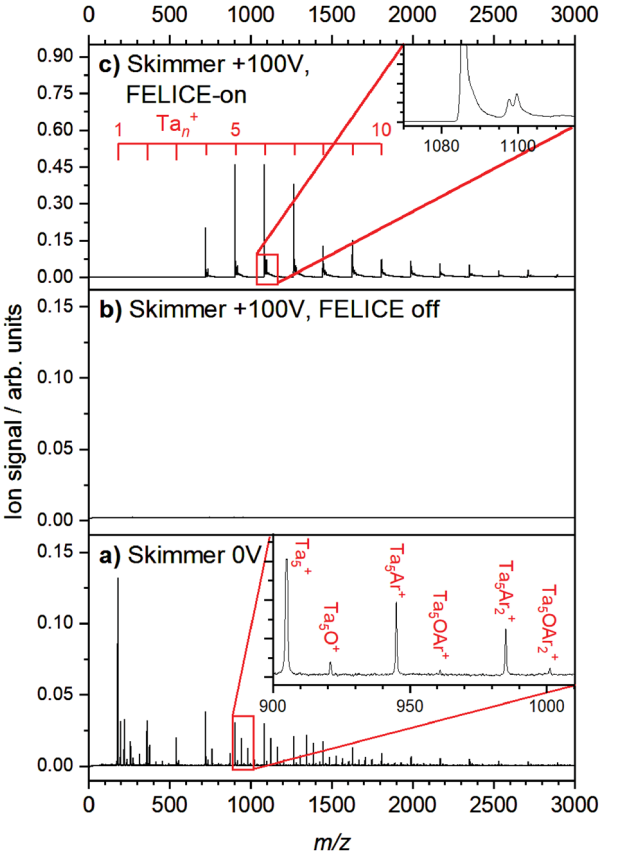

Figure 1. Tantalum cluster mass spectra produced by ablation of Ta metal in the presence of trace O_2 in 10% Ar in He. (a) Cationic species produced in the source itself, (b) shows that applying 100 V to the source skimmer prevents cations from the source entering the detection region. (c) Strong cationic cluster distribution arising from infrared ionisation of neutral Ta_nO_m clusters in the presence of the FELICE beam.

3. Results and discussion

3.1. Time-of-flight mass spectra

Figure 1 shows the representative mass spectra of $Ta_n^+/Ta_nO_m^+$ cluster ions generated (a) directly in the source itself and (c) by multiple photon infrared ionisation of *neutral* Ta_n clusters using the FELICE beam. Applying a potential of 100 V to the skimmer completely eliminates cationic clusters formed in the source region as shown in Figure 1(b). Cluster cations formed in the source region include a strong Ta^+ monomer signal and a variety of oxides and Ar-tagged clusters (incl. Ta_5O^+, Ta_5Ar^+, Ta_5OAr^+, $Ta_5Ar_2^+$ and $Ta_5OAr_2^+$ as shown in the inset). The mass spectrum in panel (a) shows decreasing ion intensities with cluster size typical of cluster growth.

The signals observed in Figure 1(c) are the focus of this study. The +100 V potential of the skimmer prevents cations from the source making it to the detection region. The ions observed are therefore produced from the effect of the FELICE beam on neutral Ta_nO_m species in the molecular beam. The spectrum shown in Figure 1(c) is a composite mass spectrum recorded as FELICE is stepped in 20 cm^{-1} intervals between 1700 and 1800 cm^{-1} but similar spectra are recorded at a wide range of wavenumbers as shown in Figure S2 which also shows the one-photon photoionisation mass spectrum at 193 nm. The $Ta_nO_m^+$ cluster size distribution in Figure 1(c) differs markedly from that in Figure 1(a) for cluster cations produced in the source and arise from multiple photon absorption followed by thermionic emission from neutral clusters. This distribution is assigned to intense Ta_n^+ and weaker $Ta_nO_m^+$ ($m = 1$–3) clusters. With typical ionisation energies of several eV (*e.g.* 5.78 eV for Ta_4) [17], it is clear that, in this FELICE energy region, very many photons (> 25) are required to reach the ionisation energy and probably many more to achieve ionisation rates exceeding 10^5 s^{-1} needed to detect ions in the experimental time window. However, the absorption of large numbers of photons is facilitated by the micro–macro pulse nature of the FELICE light source with its ps-long pulses separated by 1 ns during which IVR can occur.

The ions we detect are believed to be formed by a multiple photon ionisation followed by thermionic emission mechanism as observed previously in fullerenes [45], as well as niobium clusters [29] and metal carbides [46]

$$Ta_n + nh\nu_{IR} \rightarrow Ta_n^* \rightarrow Ta_n^+ + e^-,$$

though we cannot rule out the possibility of additional, dissociative ionisation and fragmentation processes, and their combinations.

The onset of the cluster signal from $n \geq 4$ in Figure 1(c) reflects the rapid drop in ionisation energy (IE) from the atomic Ta (7.549 eV) [47] to Ta_4 (5.78 eV) [17] and the commensurately smaller number of photons required to reach the IE. A weak odd-even intensity alternation in Ta_n^+ signals is observed in Figure 1(c) (and in similar spectra in Figure S2) which reflects the lower IE of odd n clusters due to their open shell (radical) nature. The Ta_8^+ signal is particularly low compared with Ta_7^+, Ta_9^+.

Each of the Ta_n^+ time-of-flight peaks in Figure 1(c) exhibits a significant tail towards higher m/z ratio (see inset, clearest for Ta_{5-10}^+), which is absent in Figure 1(a). We attribute this tail to delayed ionisation before or during ion extraction [16].

3.2. Infrared action spectra of Ta_n and Ta_nO clusters

The infrared multiple photon ionisation/thermionic spectra of the pure Ta_n clusters are shown in Figures S4–S6. Each spectrum is a smooth featureless band with onset in the 700–900 cm^{-1} region and increasing intensity to higher wavenumber. The intensity alternation between odd (stronger) and even (weaker) n clusters is clear in Figure S4 reflecting the relative ionisation energies. This is consistent with a mechanism involving multiple IR photon absorption followed by thermionic emission, the rise at higher wavenumber reflecting the fact that fewer photons are required to reach the IE. Spectra become less reliable beyond 1100 cm^{-1} due to the rapidly reducing fluence of the FELICE beam (Figure S1). Similar broad featureless bands have been observed have been observed previously in Ta_4^+ [7], Au_{10}^+ [41] and Co_8^+ Kr [48], and have been rationalised by the presence of low-lying electronic transitions supported by TD-DFT calculations, however the presence of such states has not been explored as part of this work.

Figure 2 shows the more interesting photoionisation spectra of Ta_nO (n = 4-13) clusters, generated by introducing an O_2 seeded gas mixture into the clustering channel via the secondary valve, and measured in the appearance channel of Ta_nO^+. Each spectrum is normalised to the intensity of the same cluster signal in the (assumed) single photon UV ionisation mass spectrum. As with the neutral clusters, the photoionisation signals are stronger for the Ta_nO^+ (n odd) clusters reflecting their lower ionisation energies. The 6.42 eV ArF UV pulse may not be appropriate for normalising for the smallest clusters whose ionisation energies are the largest. For $n > 2$ the ionisation energy (IE(Ta_3O)) is 6.22 eV (see Table S1), but for TaO it is markedly higher (8.61 eV) [23]. Panel (a) in Figure 2 shows the minimum number of IR photons required to achieve the known IE of Ta_4O, ranging from 40 to 120 depending on the photon energy.

As with the pure Ta_n clusters, each spectrum except Ta_4O exhibits a broad non-resonant increase in ion signal from > 800 cm^{-1} upwards. However, in addition, each spectrum exhibits an intense spectral band 650–700 cm^{-1} which is assigned to oxide vibrational structure. Indeed, the spectra show remarkable similarity to those of the cationic Ta_nO^+ recorded by IRMPD by way of argon-tagging [22]. Enhancement of the absorption cross section by resonance with an IR active vibrational mode facilitates IR absorption enhancing the cluster ion yield. As a result, the mass spectrum recorded with FELICE set at 675 cm^{-1} shows much stronger $Ta_nO_m^+$ ($m > 0$) oxide signals (see Figure S3, supporting information) despite significantly higher ionisation energies [49].

The similarity to the spectra of the corresponding cationic $Ta_nO_m^+$ clusters is highlighted in Figure 2 in which we indicate the spectral band positions for the bridged oxide asymmetric stretch (blue), symmetric stretch (red), and asymmetric stretch overtone (green) of the corresponding Ta_nO^+ (*i.e.* cationic) rare-gas tagging action spectra reported by Fielicke *et al.* [22]. Each spectrum includes a prominent resonant feature at *ca.* 700 cm^{-1} assigned to the symmetric stretching mode of the oxide on the surface of the cluster. This band redshifts slightly with increasing cluster size from 700 cm^{-1} for n = 4 to 650 cm^{-1} by n = 12 and there is some evidence of structure within this band, especially for the smaller clusters which may indicate the presence of multiple isomers.

Just as Fielicke *et al.* reported for the cationic cluster, in the spectrum of Ta_7O, we observe the overtone of the asymmetric oxide stretch at 870 cm^{-1}, however the current spectrum does not show signal below 500 cm^{-1} where the fundamental was observed in the earlier study. We do not observe the overtone feature reported by Fielicke *et al.* in $Ta_{10}O^+$ in our spectrum for $Ta_{10}O$, but it may be enveloped by the non-resonant feature. Both the normalised ion signal and the signal-to-noise ratio improve with larger cluster size. Notably the relative intensity of the oxide vibrational feature decreases markedly relative to the unresolved signal > 800 cm^{-1}

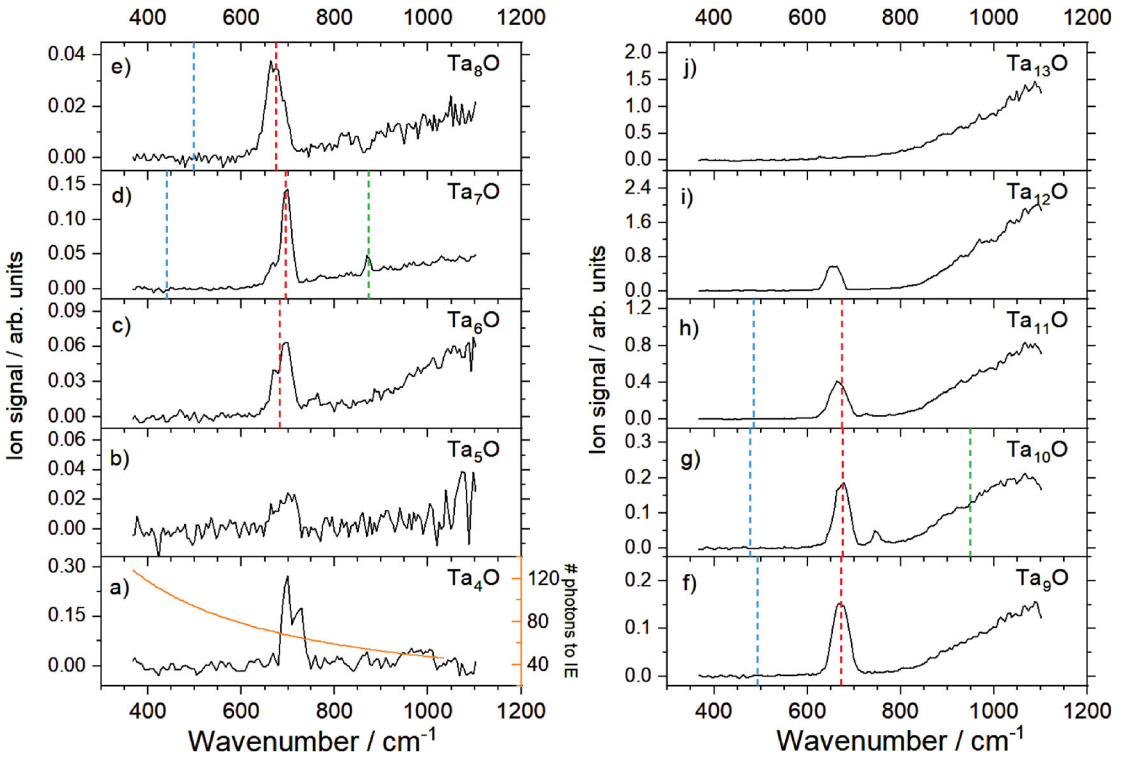

Figure 2. Multiple photon IR photoionisation action spectra of Ta_nO ($n = 4$–13) measured in the appearance channel of $[Ta_nO]^+$. Panel (a) includes a minimum number of IR photons required for non-resonant photoionisation of Ta_4O. The wavenumbers of literature vibrations of the bridged oxide asymmetric stretches, symmetric stretches and overtones of the asymmetric stretches in Ta_nO^+ are marked in blue, red, and green respectively where available [22].

as n increases with the oxide mode hard to discern in the $Ta_{13}O$ spectrum. The Ta_4O spectrum (Figure 2a) shows no evidence of a non-resonant background signal. Taken together this suggests that, in addition to the variation in ionisation energy, the increasing vibrational density of states plays a role in the ultimate efficiency of the thermionic emission process in the broad unresolved spectral feature.

Figure 3 presents a comparison between the experimental photoionisation spectra and simulated vibrational spectra for the putative ground state structures of Ta_nO ($n = 6$, 9 and 10) generated from unscaled DFT harmonic frequency calculations. All structures are low spin and, in most cases, the lowest energy binding motif for the oxygen atom is in a bridged site, which can be seen in Figure 3 (a) (Ta_6O) and (b) (Ta_9O). For $Ta_{10}O$, however, the lowest energy structure exhibits the O-atom in a three (Ta-) atom binding site (face-bound), with similar stretching modes to the corresponding bridged oxygen and the bridge binding site a slightly higher energy structure (Figure 3(c)). The observation of two bands in the spectrum may indicate the presence of a higher energy isomer/conformer (0.14 eV above the calculated global minimum) in the beam as shown. We can confidently assign the band to the stretching mode of the bridged oxygen. The secondary feature in the experimental spectrum could also be to an overtone or combination band of fundamentals $< 500\text{cm}^{-1}$ though no such band was observed in the corresponding $Ta_{10}O^+$ spectrum in this region. The face-bound structure of Ta_9O cluster lies much higher, at 0.43 eV above the putative global minimum and no such structures were found for Ta_6O.

Several of the computational spectra also show a weaker feature to the red of the main peak ($< 500\,\text{cm}^{-1}$) not observed in experiment corresponding to the asymmetric stretch of the bridged oxygen where vibrational bands were observed in previous IRMPD spectra of the cation clusters (marked in blue in Figure 2) [22]. This same mode is also present in calculated structures for Ta_6O but, as in the corresponding Nb_n spectra [29], the higher symmetry of the Ta_6 octahedron leads to negligible oscillator strength. In lower symmetry clusters the change in local charge density from O-atom motion induces a larger change in dipole moment.

3.3. Infrared spectra of Ta_nO_2 clusters

Figure 4 shows the photoionisation spectra of Ta_nO_2 clusters. These spectra exhibit similar features to the

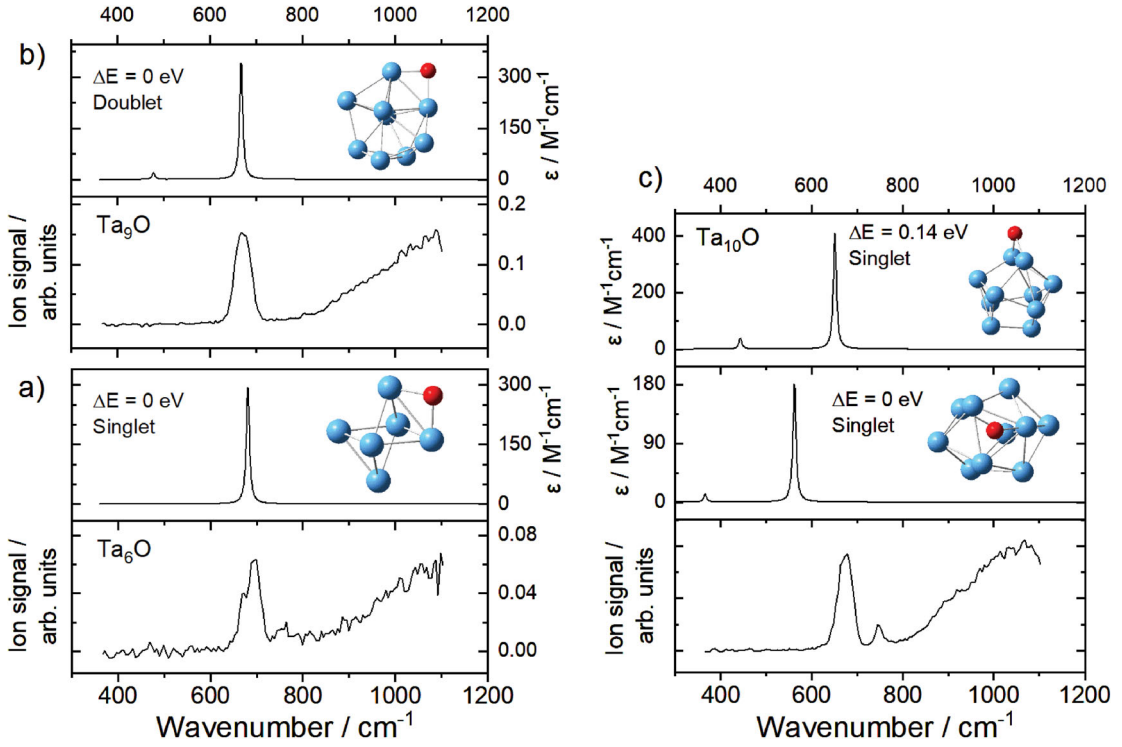

Figure 3. Comparison of experimental IR photoionisation spectra and linear IR absorption spectra of (a) Ta_6O, (b) Ta_9O, and (c) $Ta_{10}O$. Simulated spectra are generated from UB3P86/def2TZVP unscaled harmonic frequency calculations and convoluted with Lorentzian line profiles (FWHM = 8 cm^{-1}).

corresponding Ta_nO clusters with strong oxide vibrational bands and broad non-resonant features to higher wavenumber (> 800 cm^{-1}). In this case the vibrational modes comprise more complex in- and out-of-phase asymmetric oxide stretches, and a pair of in-phase symmetric oxide stretches.

Once more the spectra of the neutral clusters closely mirror those of the cationic analogues recorded in IRMPD. Figure 4 indicates vibrational features (asymmetric stretch in blue, and symmetric stretch in red) identified in the spectra of $Ta_nO_2^+$ by Fielicke *et al.* [22]. Again, we have compared unscaled harmonic frequencies from DFT calculations with experimental spectra in Figure S8 (Supporting Information). As an example, the Ta_7O_2 cluster is best described as a pentagonal bipyramid and Ta_9O_2 has two additional Ta atoms adjoining the two of the upper faces. Here the two bridged oxygen atoms are bound equatorially in both cases. In Ta_9O_2 the O-atoms sit directly opposite the two additional Ta atoms with the motion of one (at the 2–3 position) inducing a larger change in dipole moment than that in the 3–4 position. The resulting calculated frequencies of the in-phase symmetric stretches are then 684 and 653 cm^{-1} respectively, which agree very well with the experimental spectrum in which they are unresolved. As with Ta_nO, the asymmetric stretches below 550 cm^{-1} are weaker and are not observed in our spectra.

4. Summary and conclusions

Multiple photon absorption resulting in thermionic emission has been used to record the infrared spectrum of small neutral tantalum and tantalum oxide clusters with size-selectivity. Broad non-resonant absorption leads to an intense but unresolved feature in the spectra of all clusters which has a low energy threshold around 800 cm^{-1} and which grows in more strongly as the photon energy increases. In addition, the oxide clusters show clear and strong enhancements from resonance with oxide vibrational bands, most notable around 700 cm^{-1}, consistent with more efficient photon absorption. Hence, this method provides an alternative action spectroscopy in which detection of the cation cluster provides information on the structure of the corresponding neutral. The bands observed in the cluster oxide spectra are remarkably similar to those in the IRMPD studies of the corresponding cation clusters recorded by inert gas tagging [22].

Many tens of infrared photons are required to excite these clusters, thermalised in the source to T = 213–233 K, to their respective ionisation thresholds. Nevertheless, the pulse train temporal structure of the FELICE beam, coupled with the high intracavity fluence, make it near ideal for these purposes. Having been observed previously for resonant far-infrared excitation

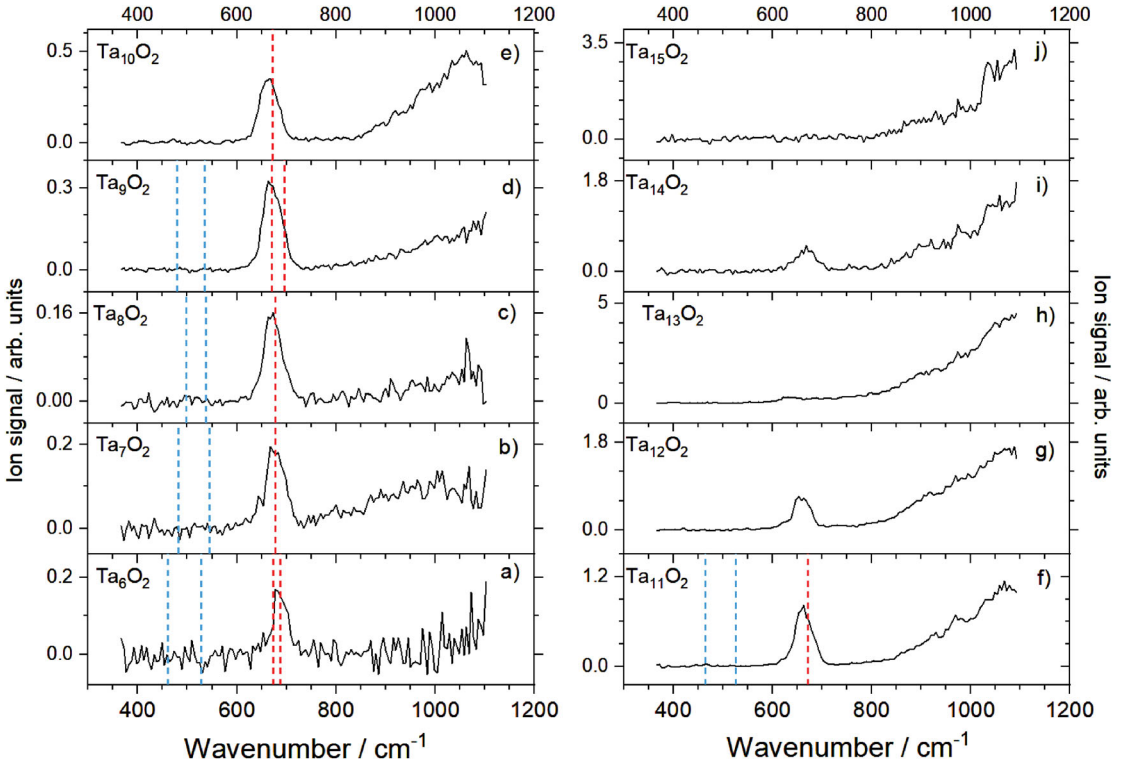

Figure 4. Multiple photon IR photoionisation action spectra of Ta_nO_2 ($n = 6$–15) measured in the appearance channel of $Ta_nO_2^+$. Blue and red dashed lines mark the frequencies of the bridged oxide asymmetric stretches and symmetric stretches, respectively, in $Ta_nO_2^+$ from Ar-tagged IRMPD studies [22].

in numerous examples [29,46,50], this multiple photon induced thermionic emission is a universal property of refractory metal clusters and offers a route to study both geometrical and electronic structures.

Acknowledgments

This work was supported by the EPSRC under Program Grant EP/T021675. PDW thanks Magdalen College, Oxford, for his Fellowship by Examination. PTR is grateful to Magdalen College, in partnership with the Clarendon Fund, for graduate funding, and PAJP is grateful to University College, Oxford, for his Bob Thomas Scholarship. The authors are grateful to the technical, research, and support staff at the HFML-FELIX facility for their professionalism and expertise. We gratefully acknowledge the Netherlands Organisation for Scientific Research (NWO) for supporting the HFML-FELIX Laboratory. We would like to thank E. Brewer for fruitful discussions on electron gun cathode materials and P. Ferrari for provision of the ArF laser used in this study. The authors would like to acknowledge the use of the University of Oxford Advanced Research Computing (ARC) facility in carrying out this work. http://dx.doi.org/10.5281/zenodo.22558

Disclosure statement

No potential conflict of interest was reported by the author(s).

Funding

This work was supported by Engineering and Physical Sciences Research Council [grant number EP/T021675].

ORCID

Peter D. Watson http://orcid.org/0000-0002-8195-1232
Ruby G. Spratt http://orcid.org/0009-0009-0065-9546
Philip A. J. Pearcy http://orcid.org/0000-0003-2784-2892
Peter T. Rubli http://orcid.org/0009-0001-4411-4048
Christian T. Haakansson http://orcid.org/0000-0003-1280-4308
Joost M. Bakker http://orcid.org/0000-0002-1394-7661
Stuart R. Mackenzie http://orcid.org/0000-0002-3166-8631

References

[1] C.L. Briant and M.K. Banerjee, *Reference Module in Materials Science and Materials Engineering* (Elsevier, 2016). doi:10.1016/B978-0-12-803581-8.02584-4
[2] H. Shelton, Phys. Rev. **107** (6), 1553–1557 (1957). doi:10.1103/PhysRev.107.1553
[3] R.O. Jenkins, Vacuum. **19** (8), 353–359 (1969). doi:10.1016/S0042-207X(69)80077-1
[4] A. Fielicke, Chem. Soc. Rev. **52** (11), 3778–3841 (2023). doi:10.1039/D2CS00104G
[5] F. Siegele, M. Tschurl, D. Schooss and U. Heiz, Chem. Phys. Chem. **26** (5), e202400513 (2025). doi:10.1002/cphc.202400513

[6] Y.M. Hamrick and M.D. Morse, J. Phys. Chem. **93** (17), 6494–6501 (1989). doi:10.1021/j100354a042; D.V. Fries, M.P. Klein, A. Straßner, M.E. Huber, and G. Niedner-Schatteburg, J. Chem. Phys. **159** (16) (2023).
[7] D.V. Fries, M.P. Klein, A. Steiner, M.H. Prosenc and G. Niedner-Schatteburg, Phys. Chem. Chem. Phys. **23** (19), 11345–11354 (2021). doi:10.1039/D0CP06208A
[8] S.W. Buckner, T.J. MacMahon, G.D. Byrd and B.S. Freiser, Inorg. Chem. **28** (18), 3511–3518 (1989). doi:10.1021/ic00317a024
[9] K.K. Irikura and J.L. Beauchamp, J. Phys. Chem. **95** (21), 8344–8351 (1991). doi:10.1021/j100174a057
[10] C.W. Bauschlicher and P. Maitre, Theor. Chim. Acta. **90** (2-3), 189–203 (1995). doi:10.1007/BF01113847
[11] L.G. Parke, C.S. Hinton and P.B. Armentrout, J. Phys. Chem. C. **111** (48), 17773–17787 (2007). doi:10.1021/jp070855z; V.J.F. Lapoutre, B. Redlich, A.F.G. van der Meer, J. Oomens, J.M. Bakker, A. Sweeney, A. Mookherjee and P.B. Armentrout, J. Phys. Chem. A **117** (20), 4115 (2013).
[12] M. Meta, M.E. Huber, M. Birk, M. Wedele, M. Ončák and J. Meyer, Faraday Discuss. **251** (0), 587–603 (2024). doi:10.1039/D3FD00171G
[13] Y. Liu, M. Ončák, T.W.R. Lewis, M. Meta, S.G. Ard, N.S. Shuman, J. Meyer, A.A. Viggiano and H. Guo, Chem. Sci. **16** (12), 5007–5016 (2025). doi:10.1039/D4SC08457H
[14] M. Meta, M.E. Huber, T. Michaelsen, A. Ayasli, M. Ončák, R. Wester and J. Meyer, J. Phys. Chem. Lett. **14** (24), 5524–5530 (2023). doi:10.1021/acs.jpclett.3c01078; M.E. Huber, T.W.R. Lewis, M. Meta, S.G. Ard, Y. Liu, B.C. Sweeny, H. Guo, M. Ončák, N.S. Shuman and J. Meyer, Phys. Chem. Chem. Phys. **26** (11), 8670 (2024).
[15] Y. Liu, M. Ončák, J. Meyer, S.G. Ard, N.S. Shuman, A.A. Viggiano and H. Guo, J. Am. Chem. Soc. **146** (20), 14182–14193 (2024). doi:10.1021/jacs.4c03192
[16] A. Amrein, R. Simpson and P. Hackett, J. Chem. Phys. **95** (3), 1781–1800 (1991). doi:10.1063/1.461026
[17] B.A. Collings, D.M. Rayner and P.A. Hackett, Int. J. Mass Spectrom. Ion Processes. **125** (2), 207–214 (1993). doi:10.1016/0168-1176(93)80043-E
[18] B.A. Collings, A.H. Amrein, D.M. Rayner and P.A. Hackett, J. Chem. Phys. **99** (5), 4174–4180 (1993). doi:10.1063/1.466114
[19] F. Dong, S. Heinbuch, S.G. He, Y. Xie, J.J. Rocca and E.R. Bernstein, J. Chem. Phys **125** (16), 164318 (2006). doi:10.1063/1.2358980.
[20] K. Hansen, Y. Li, V. Kaydashev and E. Janssens, J. Chem. Phys. **141** (2), 024302 (2014).
[21] P. Gruene, A. Fielicke and G. Meijer, J. Chem. Phys. **127** (23), 234307 (2007).
[22] A. Fielicke, P. Gruene, M. Haertelt, D.J. Harding and G. Meijer, J. Phys. Chem. A. **114** (36), 9755–9761 (2010). doi:10.1021/jp102084n
[23] J.M. Dyke, A.M. Ellis, M. Feher, A. Morris, A.J. Paul and J.C.H. Stevens, J. Chem. Soc., Faraday Trans. 2. **83**, 1555–1565 (1987). doi:10.1039/F29878301555
[24] S. Schaller, J. Seifert, G. Valtolina, A. Fielicke, B.G. Sartakov and G. Meijer, Phys. Rev. Lett. **133** (17), 173403 (2024). doi:10.1103/PhysRevLett.133.173403
[25] H. Wang, R. Craig, H. Haouari, J.-G. Dong, Z. Hu, A. Vivoni, J.R. Lombardi and D.M. Lindsay, J. Chem. Phys. **103** (9), 3289–3292 (1995). doi:10.1063/1.470263
[26] A. Fielicke, C. Ratsch, G. von Helden and G. Meijer, J. Chem. Phys. **127** (23), 234306 (2007). doi:10.1063/1.2806176
[27] A. Fielicke, C. Ratsch, G. von Helden and G. Meijer, J. Chem. Phys. **122** (9), 091105 (2005). doi:10.1063/1.1872834
[28] A. Fielicke, G. Meijer and G. von Helden, J. Am. Chem. Soc. **125** (12), 3659–3667 (2003). doi:10.1021/ja028946
[29] V.J.F. Lapoutre, M. Haertelt, G. Meijer, A. Fielicke and J.M. Bakker, J. Chem. Phys. **139** (12), 121101 (2013).
[30] V. Chernyy, R. Logemann, J.M. Bakker and A. Kirilyuk, J. Chem. Phys. **145** (16), 164305 (2016).
[31] V. Chernyy, R. Logemann, J.M. Bakker and A. Kirilyuk, J. Chem. Phys. **145** (2), 024313 (2016).
[32] A. Iskra, A.S. Gentleman, E.M. Cunningham and S.R. Mackenzie, Int. J. Mass Spectrom. **435**, 93–100 (2019). doi:10.1016/j.ijms.2018.09.038
[33] W. Fa, C. Luo and J. Dong, J. Chem. Phys. **125** (11), 114305 (2006); J. Du, X. Sun and G. Jiang, J. Chem. Phys. **136** (9) (2012).
[34] X. Li, Y. Chen, P. Basnet, J. Luo and H. Wang, RSC Adv. **9** (2), 1015–1028 (2019). doi:10.1039/C8RA09240K
[35] A.S. Chaves, M.J. Piotrowski and J.L.F. Da Silva, Phys. Chem. Chem. Phys. **19** (23), 15484–15502 (2017). doi:10.1039/C7CP02240A
[36] J. Haimson and I. Brodie, Nature. **199** (4895), 795–797 (1963). doi:10.1038/199795b0
[37] J.M. Bakker, V.J.F. Lapoutre, B. Redlich, J. Oomens, B.G. Sartakov, A. Fielicke, G. von Helden, G. Meijer and A.F.G. van der Meer, J. Chem. Phys. **132** (7), 074305 (2010); M. Haertelt, V.J.F. Lapoutre, J.M. Bakker, B. Redlich, D.J. Harding, A. Fielicke and G. Meijer, J. Phys. Chem. Lett. **2** (14), 1720–1724 (2011).
[38] P.T. Rubli, C.T. Haakansson, P.A.J. Pearcy, R.G. Spratt, J.M. Bakker, P.D. Watson and S.R. Mackenzie, J. Phys. Chem. A. **129** (26), 5810–5819 (2025). doi:10.1021/acs.jpca.5c02939
[39] F. Weigend and R. Ahlrichs, Phys. Chem. Chem. Phys. **7** (18), 3297–3305 (2005). doi:10.1039/b508541a. J.P. Perdew, Phys. Rev. B **33** (12), 8822–8824 (1986).
[40] M.J. Frisch, G.W. Trucks, H.B. Schlegel, G.E. Scuseria, M.A. Robb, J.R. Cheeseman, G. Scalmani, V. Barone, G.A. Petersson, H. Nakatsuji, X. Li, M. Caricato, A.V. Marenich, J. Bloino, B.G. Janesko, R. Gomperts, B. Mennucci, H.P. Hratchian, J.V. Ortiz, A.F. Izmaylov, J.L. Sonnenberg, D. Williams, F. Ding, F. Lipparini, F. Egidi, J. Goings, B. Peng, A. Petrone, T. Henderson, D. Ranasinghe, V.G. Zakrzewski, J. Gao, N. Rega, G. Zheng, W. Liang, M. Hada, M. Ehara, K. Toyota, R. Fukuda, J. Hasegawa, M. Ishida, T. Nakajima, Y. Honda, O. Kitao, H. Nakai, T. Vreven, K. Throssell, J.A. Montgomery, Jr., J.E. Peralta, F. Ogliaro, M.J. Bearpark, J.J. Heyd, E.N. Brothers, K.N. Kudin, V.N. Staroverov, T.A. Keith, R. Kobayashi, J. Normand, K. Raghavachari, A.P. Rendell, J.C. Burant, S.S. Iyengar, J. Tomasi, M. Cossi, J.M. Millam, M. Klene, C. Adamo, R. Cammi, J.W. Ochterski, R.L. Martin, K. Morokuma, O. Farkas, J.B. Foresman and D.J. Fox, *Gaussian 16 Rev. C.01* (Gaussian, Inc, Wallingford, CT, 2016).
[41] A.E. Green, A.S. Gentleman, W. Schöllkopf, A. Fielicke and S.R. Mackenzie, Phys. Rev. Lett. **127** (3), 033002 (2021). doi:10.1103/PhysRevLett.127.033002

[42] E.M. Cunningham, A.S. Gentleman, P.W. Beardsmore and S.R. Mackenzie, Phys. Chem. Chem. Phys. **21** (26), 13959–13967 (2019). doi:10.1039/C8CP05995K

[43] W.M. Bartczak and J. Stawowska, Struct. Chem. **15** (5), 447–459 (2004). doi:10.1023/B:STUC.0000037902.93420.28. Z.J. Wu, Chem. Phys. Lett. **370** (3), 510 (2003); S.P. de Visser, D. Danovich and S. Shaik, Phys. Chem. Chem. Phys. **5** (1), 158 (2003).

[44] M.A. Addicoat and G.F. Metha, J. Comput. Chem. **30** (1), 57–64 (2009). doi:10.1002/jcc.21026. M.A. Addicoat, S. Fukuoka, A.J. Page and S. Irle, J. Comp. Chem. **34** (30), 2591 (2013).

[45] G. von Helden, I. Holleman, G.M.H. Knippels, A.F.G. van der Meer and G. Meijer, Phys. Rev. Lett. **79** (26), 5234–5237 (1997). doi:10.1103/PhysRevLett.79.5234

[46] D. van Heijnsbergen, A. Fielicke, G. Meijer and G. von Helden, Phys. Rev. Lett. **89** (1), 013401 (2002). doi:10.1103/PhysRevLett.89.013401

[47] B. Simard, P. Kowalczyk and A.M. James, Phys. Rev. A. **50** (1), 846–849 (1994). doi:10.1103/PhysRevA.50.846

[48] K.A. Kaw, R.J. Louwerse, J.M. Bakker, P. Lievens, E. Janssens and P. Ferrari, Commun. Chem. **7** (1), 124 (2024). doi:10.1038/s42004-024-01206-2

[49] S. Smoes, F. Mandy, A.V. Auwera-Mahieu and J. Drowart, Bull. Soc. Chim. Belges. **81** (1), 45–56 (1972). doi:10.1002/bscb.19720810103. M.G. Inghram, W.A. Chupka and J. Berkowitz, J. Chem. Phys. **27** (2), 569 (1957); M. Perera, K.M. Roenitz, R.B. Metz, O. Kostko and M. Ahmed, J. Spectrosc. Dyn. **4**, 21 (2014).

[50] D. van Heijnsbergen, G. von Helden, M.A. Duncan, A.J.A. van Roij and G. Meijer, Phys. Rev. Lett. **83** (24), 4983–4986 (1999). doi:10.1103/PhysRevLett.83.4983. K. Demyk, D. van Heijnsbergen, G. von Helden and G. Meijer, A&A **420** (2), 547 (2004); G. von Helden, A.G.G.M. Tielens, D. van Heijnsbergen, M.A. Duncan, S. Hony, L.B.F.M. Waters and G. Meijer, Science **288** (5464), 313 (2000); G. von Helden, D. van Heijnsbergen and G. Meijer, J. Phys. Chem. A **107** (11), 1671 (2003).